Lappeenranta
University of Technology

Saku Levikari

GRADIENT HEAT FLUX SENSOR AND TEMPERATURE SENSOR:

A COMPARISON OF RESPONSES TO FAST HEAT TRANSIENTS

Bachelor's Thesis
LUT School of Energy Systems
Electrical Engineering

29.12.2016

Abstract

Lappeenranta University of Technology
LUT School of Energy Systems
Electricl engineering

Saku Levikari
Gradient heat flux sensor and temperature sensor: a comparison of responses to fast heat transients
2016

Bachelor's Thesis
31 pages

Examiner: Mikko Kuisma, D.Sc

Direct heat flux measurement is an important task in various fields of industry. It can also be used in a multitude of medical applications. Traditional heat flux sensors typically generate voltage by Seebeck effect. Because the generated voltage is parallel to the heat flux, the sensors usually consist of stacked thermopiles. Stacking thermopiles increases the voltage output, but also the thickness of the sensor, which in turn hampers the sensor's response time and makes it physically larger.

A new type of heat flux sensor, called the Gradient Heat Flux Sensor (GHFS) has recently been developed. The sensor is based on transverse Seebeck effect, in which the thermal emf generated is perpendicular to the heat flux. This facilitates the stacking of tilted thermopiles in direction perpendicular to the heat flux, which means that the sensor itself can be made very thin, solving many problems of the older designs.

This study was a comparative analysis between traditional temperature sensors and various Gradient Heat Flux Sensors. The sensors were heated using a pulsed diode laser, and the response characteristics were compared with each other. It was observed that traditional temperature sensors have response time from hundreds to thousands of microseconds, whereas the Gradient Heat Flux Sensors have response time in order of microseconds. Furthermore, the heat flux sensors are less affected by heat accumulation than temperature sensors.

Tiivistelmä

Lappeenrannan Teknillinen Yliopisto
LUT School of Energy Systems
Sähkötekniikka

Saku Levikari
Gradient heat flux sensor and temperature sensor: a comparison of responses to fast heat transients
2016

Opinnäytetyö
31 sivua

Tarkastaja: Mikko Kuisma, TkT

Suora lämpövuon mittaaminen on tärkeää useilla teollisuuden aloilla sekä erilaisissa tieteellisissä sovellutuksissa. Perinteiset lämpövuoanturit perustuvat Seebeck-ilmiöön, jossa lämpötilaero kahden materiaalin rajapinnan yli saa aikaan lämpövuon suuntaisen jännitteen. Riittävän jännitteen aikaansaamiseksi nämä anturit koostuvat tyypillisesti mitattavan lämpövuon suuntaisesti sarjaankytketyistä lämpöpareista. Rakenteen haittapuolena on anturin paksuuden ja lämpökapasiteetin kasvaminen, mikä hidastaa vastenopeutta ja voi vaikuttaa mitattavaan ilmiöön.

Sivuttaissuuntaiseen Seebeck-ilmiöön perustuva uudentyyppinen lämpövuoanturi on hiljattain kehitetty. Kyseisessä ilmiössä jännite muodostuu kohtisuorasti lämpövuohon nähden. Tämä mahdollistaa kallistettujen lämpöparien sarjaankytkemisen poikittain lämpövuohon nähden siten, että anturin paksuus ei kasva. Uudenlainen rakenne ratkaisee monia perinteisiin lämpövuoantureihin liittyviä ongelmia.

Tässä tutkimuksessa vertailtiin uudentyyppisten lämpövuoanturien sekä tavallisten lämpötila-anturien vasteominaisuuksia. Antureille luotiin lämpötransientti diodipulssilaserilla, ja vasteita verrattiin toisiinsa. Havaittiin, että tavallisilla lämpötila-antureilla vasteajat ovat satojen tai tuhansien mikrosekuntien luokkaa, kun taas uudentyyppisillä lämpövuoantureilla vasteajat ovat vain mikrosekunteja. Lisäksi lämpövuoanturin lämpenemisellä on vain vähäinen vaikutus mittaustulokseen.

Contents

Nomenclature

Latin alphabet

$\bar{q}, q$	Heat flux, heat flux density
$\mathbf{S}, (S_{ij})$	Seebeck tensor
$\mathbf{T}, (T_{ij})$	Transport tensor matrix describing anisotropic heat flux sensor
$\mathcal{E}_{th}$	Thermo-electromotive force
A	Surface area
b	Width of heat flux sensor (along y-axis)
D	Heat diffusivity
d	Thickness of heat flux sensor (along z-axis)
H	Heat flow
k	Thermal conductivity
l	length of heat flux sensor (along x-axis)
p	Thickness ratio of two layers in an anisotropic thermoelement
P_{abs}	Absorbed power (of laser radiation)
Q	Thermal energy, heat
r	Thermal resistivity
S	Seebeck-coefficient
S_0	Sensitivity coefficient of heat flux sensor
T	Temperature
t	Time
z	Optical axis of measurement setup
A, B	Materials with different thermal and electrical conductivities

Greek alphabet

α	Angle (tilt, of thermoelement plates)
ρ	Mass density
σ	Electrical conductivity

Subscripts

$\parallel, \perp$	Parallel, perpendicular
abs	Absorbed
d	Delay
f	Fall (time)
i, j	Matrix indices
opt	Optimized
q	Heat current
r	Rise (time)
th	Thermal
x, y, z	Components along axes

Abbreviations

junc	Junction
ref	Reference

1 Indroduction

Heat flux sensor has many practical applications in industry. Its uses range from industrial boilers and electric machines to various medical applications. Some examples of practical applications of heat flux sensors are fluid flow monitoring (via changes in thermal conductivity or temperature); waste heat recovery; electric motors (Jussila et al., 2013); studying combustion processes inside a diesel engine (Sapozhnikov et al., 2006); monitoring of heat flow from human body (Tunnell et al., 2002); light sensing applications (Kyarad and Lengfellner, 2004); thermal imaging (Kanno et al., 2014); environmental studies and agriculture (Sapozhnikov et al., 2008).

The main advantages of a heat flux sensor compared to a conventional thermometers are faster response for temperature transients and the ability to measure the direction of the heat flow. With the heat flux sensor, it is also possible to detect change in thermal conductivity of a medium, even if the temperature difference over the sensor remains the same.

Temperature T describes the kinetic energy of atoms at a certain point. It is a scalar field, i.e. it has magnitude, but no direction. On macroscopic level, two objects are defined to be in equal temperature when there is no thermal energy (Q) exchange between them. Vice versa, when there is a temperature difference between two objects, thermal energy is exchanged between them (assuming that the objects are not ideally thermally isolated). Thermal energy, or *heat*, is transported as *heat current* H, $H = \frac{dQ}{dt}$ $\left([H] = \frac{\mathrm{J}}{\mathrm{s}} = \mathrm{W}\right)$, by the means of conduction, convection, radiation, or as a combination of these. (Young and Freedman, 2008)

Heat flux $\bar{q}$ is the heat current through a surface. It is a vector field, i.e. it has both magnitude and direction. The magnitude of heat flux is called *heat flux density*, which is the heat current per unit area. Heat flux is proportional to temperature gradient ∇T and to the thermal conductivity k of the medium. If the temperature distribution, thermal conductivity and dimension of an object are known, an estimate for the heat flux inside the object can be calculated. However, in many modern applications, it is necessary to get direct information about the heat transformation through an object. This can be achieved using a heat flux sensor.

Voltage generation by heating bimetallic junction was discovered by T. J. Seebeck in 1821. In 1834, J. Peltier discovered heating/cooling effect by applying electrical current into a bimetallic junction. The Peltier effect is the opposite to the Seebeck effect, and has similar physical basis. In 1855, the dependence of these two effects was recognized by W. Thomson (Goldsmid, 2010). Anisotropic thermoelectric effects in single-crystal bismuth were studied already in 1927 by Boydson; earlier work in this field has been done by Perrot, Lownds, Jordan, Borelius, Lindth and Bridgman (Boydston, 1927). The theoretical basis for thermoelectricity in inhomogeneous,

anisotropic media was established in 1953 by Charles A. Domenicali.(Domenicali, 1953) The first transverse-Seebeck-based heat flux sensors based on single crystal bismuth were created by Divin (Sapozhnikov et al., 2008). Research for developing anisotropic thermoelectric devices was started in 1964 by A. G. Samoilovich, and was studied extensively at Chernovtsy State University, Ukraine (Snarskii et al., 1997).

Several different types of q-sensors based on artificial anisotropy have been developed. Zahner et al. have developed a heat flux sensor based on sintered copper/constantan multilayer structures (Zahner et al., 1999). A high-temperature heat flux sensor based on 10 series-connected brass-steel junctions was made at the Polytechnic Institute of Virginia by Sujay (Sujay, 2005). Quin et al. created a heat flux sensor based on $SrTiO_3/SrTi_{1-x}Nb_xO_3$ multilayer films (Qin et al., 2014). Fischer et al. constructed a q-sensor based on chromel-constantan multilayers (Fischer et al., 2004). Kanno et al used sensors made of multilayered Bi/Cu and $Bi_{0.5}Sb_{1.5}Te_3$/Ni (Kanno et al., 2014).

In comparison to a temperature sensor (or *T-sensor*), a heat flux sensor (or *q-sensor*) is a device that measures the heat flow through the sensor itself instead of temperature. Commercial heat flux sensors are typically based on thermocouples, which utilize Seebeck effect to generate thermoelectric voltage (Sapozhnikov et al., 2008).

All q-sensors in this study are based on *transverse Seebeck effect*. These sensors are constructed from both thermally and electrically anisotropic materials, which generate thermo-electromotive force $\mathcal{E}_{th}$ perpendicular to the heat flux. The $\mathcal{E}_{th}$ generated in transverse Seebeck effect is based on the same physical phenomenon as in "ordinary" Seebeck effect: in two materials A and B, with different conductivities, charge carriers (electrons) have different energies. When a junction of these conductivities is heated, electrons on one side of the junction with the lower energy can pass to the other side of the junction, where the electrons have higher energy. The result is imbalance within the charge carriers, which generates electromotive force. (Goldsmid, 2010). In isotropic medium, the voltage generated is parallel to the interface of materials A and B. Because A and B have different thermal conductivities, the temperature gradient is also parallel to the interface of A and B. In anisotropic media, the temperature gradient is "bent" between the interface of A and B, resulting in both parallel and perpendicular components of ∇T. The voltage generation by the perpendicular component of the heat flux is called the transverse Seebeck effect.

1.1 Goal of this study

The goal of this study is to compare the heat transient responses of GHFSs and conventional temperature sensors. Differences between these responses are also com-

pared. The sensors' heat transient responses are evaluated by the output signals' delay, rise and fall times. Two methods were used to evaluate the response properties of the sensors:

Theoretical method
A simplified physical model of a heat flux sensor is constructed. Equations for voltage generation and heat transfer are presented and response characteristics of q-sensor are evaluated based on these equations.

Experimental method
The output differences of q- and T-sensors are studied. The sensors are heated by laser pulses of 10 μs temporal duration using a pulsed diode laser. The experimental results are compared with the theoretical models.

1.2 Research questions

The research questions of this thesis are:

- Does the heat flux sensor have a faster response for temperature transient than the temperature sensor?
- What causes the difference between the response times?
- How does the accumulation of thermal energy contribute to the signals generated by q- and T-sensors?
- How does the thermal capacity affect the operation of a heat flux sensor?

The object of interest is the correlation between the thermo-emf produced by the heat flux sensor and the temperature gradient of short temporal duration, produced using a pulsed laser.

2 Physical model of gradient heat flux sensor

Heat flux $\bar{q}$ is a vectorial quantity that describes the *rate of heat energy transfer per unit surface per unit time*. Heat flux is defined by Fourier's law as a function of thermal conductivity k and temperature gradient ∇T

$$\bar{q} = -k\nabla T,\ [\bar{q}] = \frac{W}{\mathrm{m}^2}\hat{x} \tag{2.1}$$

where k is either a scalar value or a tensor. The heat flux density q is the heat current per unit area. Heat flow, or *heat rate*, $H = \frac{dQ}{dt}$, is the heat flux through a given surface A,

$$H = \iint_A \bar{q} \cdot d\bar{A} \tag{2.2}$$

or $H = qA$, if $\bar{q} \parallel d\bar{A}$. Heat flux can be measured indirectly utilizing Fourier's law,

$$\bar{q} = \frac{k\Delta T}{d} \tag{2.3}$$

where d is the thickness of the surface the heat flux passes through. Heat flux can also be measured directly using a heat flux sensor, which typically generates thermoelectric emf $\mathcal{E}_{th}$ by Seebeck effect. The $\mathcal{E}_{th}$ generated is parallel to the heat flux: in order to generate measurable voltages, a traditional heat flux sensor consists of thermopiles stacked in the direction of the measured heat flux. This limits both the minimum thickness of the sensor, and the response time because heat diffusivity is proportional to the thickness squared (Fischer et al., 2004).

The experiments in this study were made using gradient heat flux sensors. These sensors are based on anisotropic thermoelements (AT) which generate thermo-emf perpendicular to external heat flux. Such thermoelements are typically constructed by layering metals or semiconductors with different thermal and electrical conductivities at an angle α (fig. 2.2). The ATs are then connected in series (fig. 2.1), creating a plate-like structure that can be made much thinner than traditional heat flux sensors.

A typical anisotropic thermoelement is made of two different isotropic materials A and B. These materials can be described by their bulk properties S, σ, ρ, k and r. Layering these materials as A|B|A... results in anisotropic structure, for which a general transport tensor $\mathbf{T_0}$ can be formulated as

$$\mathbf{T_0} = \begin{pmatrix} T_\parallel & 0 & 0 \\ 0 & T_\parallel & 0 \\ 0 & 0 & T_\perp \end{pmatrix}. \tag{2.4}$$

(Mann, 2006), (Vemuri and Bandaru, 2013). For an AT described in fig 2.2, a

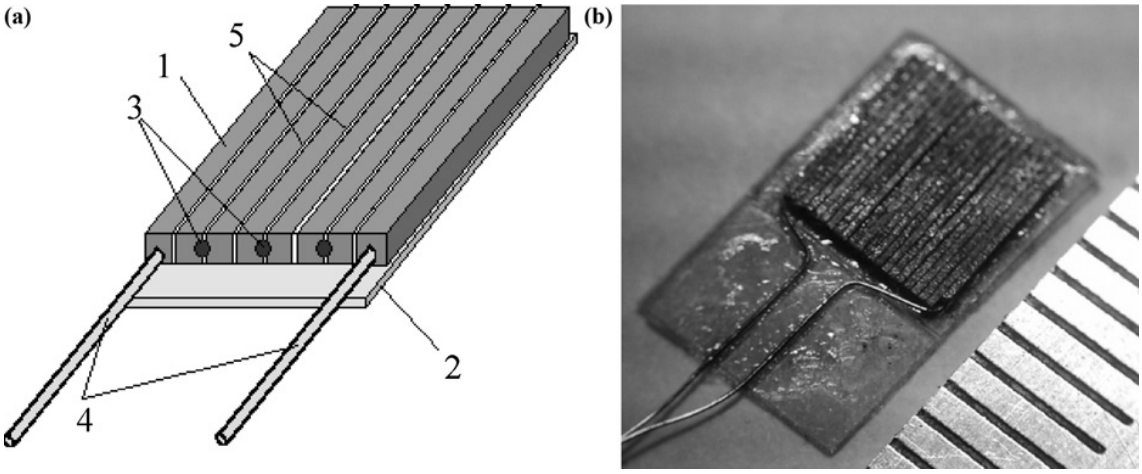

Figure 2.1: Schematic (a) and general view (b) of a battery GHFS (next to mm scale). 1 – AT; 2 – mica substrate; 3 – pure bismuth soldering junctions for electrical connection between ATs; 4 – current leads; 5 – teflon or mica insulation gaskets. (Sapozhnikov et al., 2008)

general transport tensor $\mathbf{T}$ can be formulated by rotating (2.4) around the y-axis by an angle α (Vemuri and Bandaru, 2013); this corresponds to tilting the layered structure as A/B/A... by the angle α (fig. 2.2), resulting in rotated transport tensor (Fischer et al., 2004):

$$\mathbf{T} = (T_{ij}) = \begin{pmatrix} T_\parallel \cos^2\alpha + T_\perp \sin^2\alpha & 0 & \frac{1}{2}\left(T_\parallel - T_\perp\right)\sin 2\alpha \\ 0 & T_\parallel & 0 \\ \frac{1}{2}\left(T_\parallel - T_\perp\right)\sin 2\alpha & 0 & T_\parallel \sin^2\alpha + T_\parallel \cos^2\alpha \end{pmatrix}, \tag{2.5}$$

where

$$(T_\parallel, T_\perp) = (S_\parallel, S_\perp),\ (\sigma_\parallel, \sigma_\perp),\ (\rho_\parallel, \rho_\perp),\ (k_\parallel, k_\perp) \text{ or } (r_\parallel, r_\perp)$$

A tilted AT has different thermal and electrical conductivities parallel and perpendicular to the surface. Aside from layering materials A and B at an angle, similar kind of anisotropy occurs naturally in some substances, such as single-crystal bismuth. The thermal anisotropy causes the heat flux to change direction inside the AT. Because the heat flux is not parallel to the z-axis, the resulting temperature gradient (2.1) comprises of longitudinal and transverse components. The transverse gradient component results in transverse voltage which can be measured.

For an anisotropic, layered object, the following coefficients for Seebeck effect and thermal conductivity can be constructed by utilizing the Kirchoff's laws: (Fischer et al., 2004):

$$\begin{aligned} S_\parallel &= \tfrac{S_A\sigma_A + pS_B\sigma_B}{\sigma_A + p\sigma_B}, & S_\perp &= \tfrac{S_A k_B + pS_B k_A}{pk_A + k_B} \\ k_\parallel &= \tfrac{k_A + pk_B}{1+p}, & k_\perp &= \tfrac{k_A k_B (1+p)}{pk_A + k_B} \end{aligned} \quad . \tag{2.6}$$

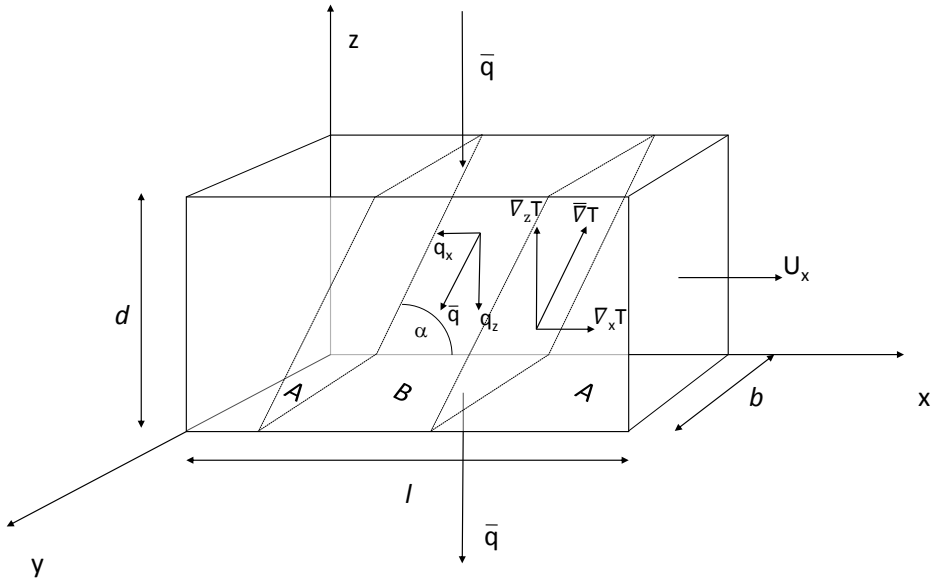

Figure 2.2: Illustration of an anisotropic thermoelement made of materials A and B.

To simplify the model of AT, it is assumed that

- A single thermoelectric element is long, i.e. $l >> d$.
- The heat flux is perpendicular to the sensor surface: $\bar{\nabla}T = \nabla_z T\hat{z}$

The approximation $\bar{\nabla}T = \nabla_z T\hat{z}$, as made by Reitmaier et al. (2010), is valid as a macroscopic interpretation for the temperature drop along the sensor, even though the actual voltage generation inside the sensor is facilitated by the transverse component $\nabla_x T\hat{x}$ of the temperature gradient.

By assuming $l >> d$, the diffusion of heat in the sensor can be approximated by the one-dimensional heat diffusion equation (Zahner et al., 1999)

$$\frac{\partial T}{\partial t} = D\frac{\partial^2 T}{\partial z^2}, \tag{2.7}$$

where D is the thermal diffusivity:

$$D = \frac{k}{\rho_m c} \tag{2.8}$$

When the thermoelectric element is heated on one side using a laser, the heat is primarily transported by radiation. Ignoring the effects of Peltier and Joule heating and assuming that the heat flows in the z-direction only, the temperature gradient

in the AT becomes

$$\bar{\nabla}T = \left(0, 0, \frac{\partial T}{\partial z}\right) = \left(0, 0, \frac{\Delta T}{d} l\right) = \left(0, 0, \frac{q}{k_{zz}}\right), \tag{2.9}$$

The equation above assumes that the temperature drop is linear along the z-axis. This is a reasonably good steady-state assumption (Lienhard IV and Lienhard V, 2015), and used here because the sensor structure is thin in the z-direction. A more accurate results could be obtained using (2.7). The $\mathcal{E}_{th}$ per unit length generated by a single AT is

$$\mathcal{E}_{th} = \mathbf{S}\bar{\nabla}T \tag{2.10}$$

where $\mathbf{S}$ is the Seebeck tensor, constructed as in (2.5) using Seebeck-coefficients $S_\parallel$ and $S_\perp$. Considering a steady-state-situation, using (2.9) it is obtained that the thermo-electric emf of a single AT is

$$\mathcal{E}_{th} = \mathbf{S}\bar{\nabla}T = \begin{pmatrix} S_{xx} & S_{sy} & S_{xz} \\ S_{yx} & S_{yy} & S_{yz} \\ S_{zx} & S_{zy} & S_{zz} \end{pmatrix} \begin{pmatrix} 0 \\ 0 \\ \nabla_z T \end{pmatrix} = \begin{pmatrix} S_{xz}\frac{\partial T}{\partial z} \\ 0 \\ S_{zz}\frac{\partial T}{\partial z} \end{pmatrix} \tag{2.11}$$

hence the output voltage of the q-sensor is

$$U_x = \mathcal{E}_{th} l = S_{xz}\frac{\partial T}{\partial z} = S_{xz}\frac{\Delta T}{d} l = \frac{1}{2}\left(S_\parallel - S_\perp\right)\sin(2\alpha)\left(\frac{\Delta T}{d} l\right). \tag{2.12}$$

The power $P_{\text{abs}} = qlb$ absorbed by q-sensor can be calculated from the output voltage. Heat current density (per area A) forms a temperature gradient in the z-direction:

$$\frac{P_{\text{abs}}}{A} = \nabla_z T k_{zz} \tag{2.13}$$

which generates voltage in the x-direction:

$$U_x = \frac{S_{zx}}{k_{zz}}\frac{P_{\text{abs}}}{l} = \frac{1}{2}\left(S_\parallel - S_\perp\right)\frac{\sin(2\alpha)\, P_{\text{abs}}}{k_\parallel \sin^2\alpha + k_\perp \cos^2\alpha}\frac{l}{A} \tag{2.14}$$

(Fischer et al., 2004), (Reitmaier et al., 2010). The Seebeck-coefficients $S_\parallel$ and $S_\perp$ can be considered as bulk properties listed in literature, when the q-sensor is based on single material, e.g. single-crystal bismuth. If the q-sensor is based on multilayer structure, these properties can be defined as in (2.6).

2.1 Sensitivity of the Gradient Heat Flux Sensor

The volt-watt-sensitivity S_0 for AT is obtained from

$$S_0 = \frac{S_\parallel k_\perp - S_\perp k_\parallel}{2 k_\parallel k_\perp b} \tag{2.15}$$

(Snarskii et al., 1997), or on a macroscopic level,

$$S_0 = \frac{\mathcal{E}_{th}}{q_z A}. \tag{2.16}$$

(Sapozhnikov et al., 2008). In the absence of standard heat flux sensors, the calibration for S_0 has to be done in order to obtain absolute values for heat flux. Sapozhnikov et al. (2012) have proposed a calibration method in which the output voltage U_x is compared with heat flow through the surface of the sensor $P = q_z A$. The q-sensor is heated with a standard heater with current I and voltage drop U, so that

$$U_x \propto P = q_z A = UI \tag{2.17}$$

(Sapozhnikov et al., 2012). The $\mathcal{E}_{th}$ generated by a single AT is heavily dependent on its thermoelectric anisotropy $\Delta S = S_{\parallel} - S_{\perp}$, along with its thickness ratio p, (Reitmaier et al., 2010) and tilt angle α,

$$\alpha_{\text{opt}} = \pm \arctan \sqrt{\frac{k_{xx}}{k_{zz}}}, \tag{2.18}$$

(Sapozhnikov et al., 2008). The optimal thickness ratio p_{opt} depends on the materials used.

2.2 Time resolution of the Gradient Heat Flux Sensor

The response time of a heat flux sensor depends on its thickness (Sapozhnikov et al., 2008), (Reitmaier et al., 2010), assuming the delay caused by signal amplification is ignored. The time constant τ of an AT can be approximated by (Snarskii et al., 1997)

$$\tau = \frac{0.4 d^2}{D}, \tag{2.19}$$

assuming the Peltier effect is weak. When a q-sensor is irradiated with a laser pulse of $\sim 10^{-8}$ s in duration, the layer of the q-sensor in which the $\mathcal{E}_{th}$ is generated (i.e. where the temperature difference occurs) is less than a micrometer in thickness (Sapozhnikov et al., 2008). This facilitates thin structure and fast heat transient response.

2.3 Comparison with temperature sensors

The main difference between heat flux sensor and temperature sensor is that the output signal of heat flux sensor does not directly depend on the mean temperature of the sensor itself, but on temperature difference. Difference in temperature creates flow of heat, hence the name heat flux sensor. The temperature sensors used in this study are based on two different principles of measuring temperature. K- and T-type thermocouples are based on two bimetallic junctions connected by wires. The

temperature difference between these junctions leads to thermal emf which can be measured. The $\mathcal{E}_{th}$ generated by conventional thermocouples is

$$\mathcal{E}_{th} = \int_{T_{ref}}^{T_{junc}} (S_1 - S_2)\, dT = \int_{T_{ref}}^{T_{junc}} \Delta S dT, \tag{2.20}$$

where T_{junc} is the temperature of the sensing junction of the thermocouple, and T_{ref} is the reference temperature at the other end of the wires, where the voltage is measured from (Scervini, 2009). PT100 is a resistance thermometer, which is based on the change of resistivity in platinum as a function of temperature. The PT100 has a resistance of 100 Ω at 0°C, and a 1°C change of temperature will change the resistance by 0.384 Ω (pic, 2015). An accurate measurement of resistance is facilitated by connecting the PT100 in a Wheatstone bridge configuration.

3 Measurements

For determining the response characteristics of the q- and T-sensors, a pulsed diode laser was chosen as the heat source. The reason for this was the laser's ability to create step-like heat transients. When a sensor is heated by a laser, the heat is transported by radiation. This eliminates any delay caused by conduction or convection. Another option for generating heat flux with conductive heat transfer is a resistor fed with short bursts of high current. This method was abandoned because of relatively slow heating of the resistor and difficulties with providing a solid connection between the resistor and q-sensor for repeatable measurements. A third, convection-based heat source for a q-sensor would be a shock tube, as used by Bobashev et al. (2008).

3.1 Measurement equipment

3.1.1 Sensors

In this study, several transverse Seebeck-based heat flux sensors of different types were used. A selection of several temperature sensors were used for reference. The heat flux sensors used in this study were:

B1: A sensor based on single-crystal bismuth with size of 2.0 mm by 2.5 mm

B2: A sensor based on single-crystal bismuth with size of 10.0 mm by 10.0 mm

HGHFS: A high-temperature heat flux sensor attached into a hex bolt, size 6.5 mm by 7.0 mm

$\mathbf{HGHFS_0}$: A high-temperature heat flux sensor without a hex bolt, size 6.5 mm by 7.0 mm

Si: A silicon-based heat flux sensor, size 5.0 mm by 7.0 mm

The temperature sensors used in this study were:

PT: A PT100 thermistor in a Wheatstone bridge configuration

K: A thermometer based on a K-type thermocouple

T: A thermometer based on a T-type thermocouple

Figure 3.1 shows all the sensors alongside a scale. The measurements were made in room temperature, $T \approx 20°\mathrm{C}$.

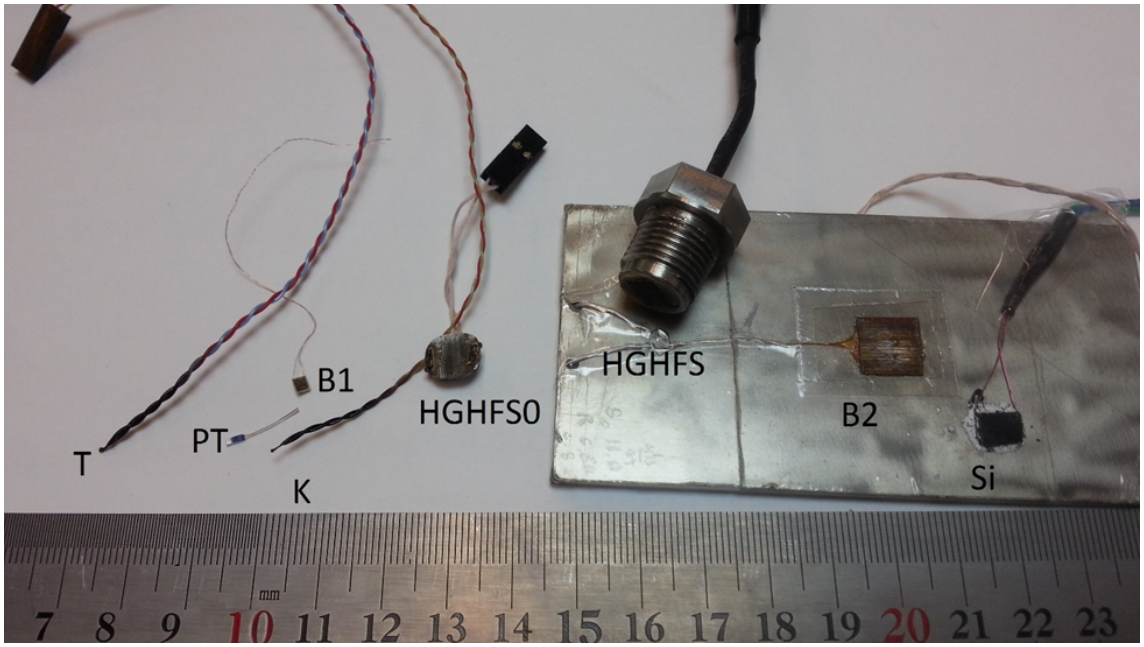

Figure 3.1: The heat flux- and temperature sensors used in this study.

3.1.2 Laser

The heat transients were generated using Cavilux Cavitar pulsed diode laser with wavelength of $\lambda = 680\,\text{nm}$. The peak power of the laser is several hundreds of watts, and the pulse shape in time-intensity plane is approximately rectangular. The repetition rates, durations and patterns of the laser pulses were configured using CAVILUX Control Software. The laser was set on full power on a separate CAVILUX Control Unit. Pulse durations were adjustable within the interval of 40 ns - 10 μs. The repetition rate was set to 9,9 Hz, which was chosen in order to facilitate the detection of individual pulses even with the slowest sensors of the test group. The laser was placed approximately $5 - 15\,\text{mm}$ away from a sensor and the laser pulse was aimed straight at the sensor without any optical isolation. The rectangular pulse shape of the laser is not a proper step input for the sensor, but if the response time of the sensor is in order of 1/10th of the excitation time, the response can be considered a step-like (Sapozhnikov et al., 2008).

3.1.3 Oscilloscope

The heat transient responses of the sensors were measured using a Keysight InfiniiVision MSO-X 4104A oscilloscope, which has a bandwidth of 1 GHz and sample rate of 5 GSa/s. A high bandwidth, high sample rate oscilloscope was required to accurately measure the response characteristics of q-sensors, because the timescales are in order of $< 1\,\mu$s. The sensors were connected to the input of the oscilloscope either directly or through an amplifier. Measurements were made on several time scales to focus on the sensor's rise time, fall time, or accumulation of heat in the

sensors. The measurement data was processed in Matlab.

3.1.4 Amplifiers

The sensors were connected into the oscilloscope through an amplifier for improved signal-to-noise ratio. The gain factors for each of the sensors are presented in table 3.1. The amplifiers were encased in aluminum cases for shielding.

Table 3.1: Gain factors used in the measurements

Sensor	B1	B2	Si	PT	K	T	HGHFS	$HGHFS_0$
Gain	830	100	11,7	830	830 (set 12: G=100)	830	830	830

The amplifiers comprised of two cascade-connected op-amps. Measurement and amplification of heat flux sensor have been discussed in depth by Niukkanen (2013) and Heiskanen (2015).

3.2 Description of test setup

The measurement setup was constructed on a table as shown in 3.2. During the measurements, the sensors were attached onto an aluminum plate with either silicone paste or blu-tack. The amplifier was placed behind the plate. The leads from the sensor to the amplifier were shielded using copper tape. A small hole for the leads was made in the casing. A BNC connector was attached to the casing to connect the amplifier to the oscilloscope. Initial design was 4 individual amplifiers encased in one casing, but this was abandoned due to oscillation problems.

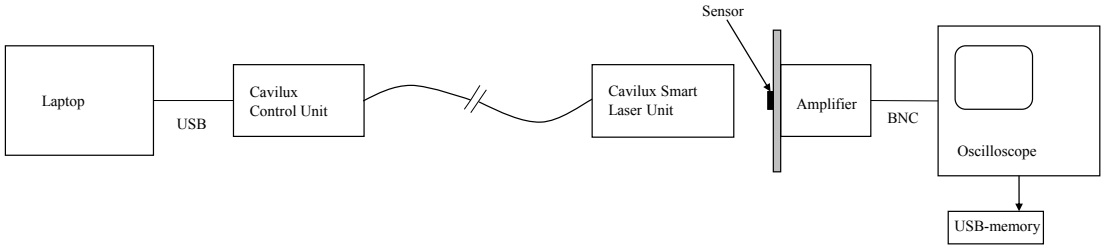

Figure 3.2: Illustration of the test setup.

The measurements were made in 25 different sets, in each of which 1-4 sensors were used. Each set was divided into 5-16 measurements. The measurements in each set were made using time scales of 20 s, 2 s, 200 ms, 2000 μs and 50 μs on the oscilloscope.

4 Results and discussion

4.1 Theoretical evaluation

The q-sensors can be expected to have faster response for heat transients than the T-sensors because of the different operational principles of the sensors. As seen from (2.13), the voltage generated by an AT is proportional to the length l of the thermoelement, and inversely proportional to the thickness d of the thermoelement (2.12), when steady-state situation is assumed. Because the q-sensors are constructed by wiring the ATs in series, the heated surface area equals to a long total length l_{tot},

$$l_{tot} = \sum_{i=1}^{n} l$$

where n is the number of thermoelements in the heated area. This facilitates the relatively immediate voltage production when the q-sensor is irradiated by laser beam. The output of the T-sensors, however, depends not on the surface temperature but the mean temperature of the sensors. With thermocouples, the voltage output is proportional to the overall (mean) temperature difference between the bimetallic sensing junction and the reference junction of the sensor, as in eq. (2.20), whereas the resistivity of PT100 changes with the overall temperature of the resistor.

The materials of the q-sensor affect the thermal diffusivity D. The diffusivity of heat along the z-axis affects the temperature gradient, which is directly related to the voltage output of the sensor. Maximizing diffusivity D and minimizing thickness d will yield shorter time constant τ, as in (2.19).

4.2 Measurements using laser-generated heat transients

The response speed of each sensor was analyzed by subjecting a sensor to a 10 μs laser pulse and measuring the sensor's voltage output. In Table 4.1, the response of each sensor is characterized by delay (t_d), rise (t_r) and fall time (t_f), corresponding to time the sensor's output takes to change from 0 . . . 10 %, 10 . . . 90 % and 90 . . . 10 %, relative to the maximum output voltage. The measurements noise was assumed to be unbiased, so lower and upper states for t_d, t_r and t_f were defined as mean values of the noisy output signal. The step response of a q-sensor can be considered a 1st order system response, as in eq. (2.19). As the input signal duration was limited by the hardware, the results in Table 4.1 are not true step responses. However, in cases where the observed rise time is shorter than the pulse duration (B1, B2, Si), the response is considered step-like. The observation model for 1st order system step response is

$$U(t) = K\left(1 - e^{-t/\tau}\right) + v, \tag{4.1}$$

where K is the gain factor of the system, τ is the time constant and v is random error contained within the observations.

Time constants τ were defined for sensors B1 and B2 by fitting the model (4.1) into the measurement data. The laser pulse responses and fitted curves are shown in Figs. A.1 and A.2. As seen from these figures, the model (4.1) describes the laser pulse response of these sensors reasonably well. For the Si-sensor, the time constant was manually estimated from the measurements, as the model in (4.1) fails to accurately describe the output of the sensor. For sensors with t_r longer than the laser excitation time (HGHFS, $HGHFS_0$, PT, K and T), 1st order system is not a suitable model; therefore, there are no time constants defined for these sensors.

Table 4.1: The determined delay-, rise-, and fall times for each sensor stimulated with 10μs laser pulse.

Sensor	Delay time $t_d(\mu s)$	Rise time $t_r(\mu s)$	Fall time $t_f(\mu s)$	Time constant $\tau(\mu s)$
B1	0.3	6.5	344.0	3.1
B2	0.2	6.6	514.5	3.2
Si	0.08	1.1	9.3	0.4
HGHFS	14.6	19.6	7300 (extrapolated)	-
$HGHFS_0$	-	36	2600 (extrapolated)	-
PT	1000	3000	7000	-
K	55(avg)	700(avg)	-	-
T	-	-	-	-

From table 4.1 it can be seen that the Si-based sensor has the fastest response (shortest delay and rise time) for the laser pulse. The bismuth-based sensors have both approximately equally fast response. The high-temperature sensors have notably slower response for the laser pulse, and also longer fall time. The fall times of HGHFSs' are extrapolated from the measurement data.

No unambiguous constants were defined for the T-type-thermocouple because the output voltage was overshadowed by measurement noise. The measurement data of the K-type thermocouple was also noisy, so t_d and t_r were estimated exposing the sensor to repeated pulses and taking the average of the output. t_f for high-temperature heat flux sensors are linearly estimated from the measurements, and thus may deviate from true values by several thousands of microseconds.

4.3 Response characteristics of q- and T-sensors

From the measurement data and figures 4.1 and 4.2, it is observed that the heat flux sensor have heat transient response several orders of magnitude faster than the T-sensors. Bismuth- and silicon-based q-sensors have rise time in order of microseconds, whereas high-temperature heat flux sensors have rise time in order tens of microseconds. The temperature sensors used in this study have rise time in order of hundreds or thousands of microseconds. It must be noted that when using

amplifiers with gain factor $G \sim 1000$, the rise time of the amplifier is in order of hundreds of microseconds. This may partially explain the slow measured response of high-temperature sensors, compared to those based on bismuth or silicon.

Q-sensors' output signal also settles back to its original state faster than T-sensors'. A common trait in the measurement data of the q-sensors (excluding the HGHFS-type sensors, figures 4.3 and 4.4) is that the voltage output of the sensor reaches its maximum at the moment when the laser pulse ends (see 4.7), meaning that the response time is in order of microseconds. With the T-sensors, the time to reach the maximum output is in order of milliseconds (table 4.1).

When temperature gradient has short temporal duration, the response time of a heat flux sensor appears to be dependent on the construction and materials used in the sensor, rather than its thickness and other physical dimensions. This implies that the voltage generation in ATs during short duration heat gradients is mainly a surface phenomenon. These results agree with the calculations by Sapozhnikov et al. (2008): the $\mathcal{E}_{th}$ is generated in the surface of a q-sensor, within the depth of ~ 1 μm, whereas the thicknesses of the sensors are in order of 1 mm, which is thick compared to the effective thicknesses of the q-sensors.

4.4 Sensitivity comparison

Using a 10 μs laser pulse, the sensor B2 produced a maximum voltage of 20.5 mV, whereas using B1 the maximum voltage was approximately 1.1 mV. Considering that the surface area of B2 is approximately 20 times the area of B1, B1 and B2 have roughly the same voltage-per-area -sensitivity (as in (2.16)): with a 10 μs pulse, B1 produces 0.22 mV/mm^2 and B2 produces 0.205mV/mm^2. The peak voltage generated by the HGHFS-sensors was about $6 - 7$ μV, which yields approximately $0.13 - 0.15$ μV/mm^2. For the Si-sensor, the maximum voltage can be interpolated as approximately 30 mV, which corresponds to 0.86mV/mm^2. This is only a rough approximation, because the voltage output of this sensor was observed to be dependent on the rotational angle (along the z-axis) of the sensor. In general, shorter response times were observed for GHFSs with high volt-watt-sensitivity.

The temperature sensors used are not directly comparable with the heat flux sensors by their voltage-per-area-sensitivity. With K- and T-type thermocouples, individual pulses couldn't be distinguished from the measurement noise. Cleaner measurement data was obtained by taking averaging measurements from the repeated pulses, but this prevented the observation of the temperature change caused by an individual pulse. The poor heat transient response of the K- and T-type sensors is probably related to the small surface area of the bimetallic junction in these sensors, resulting in small absorbed power in comparison to the heat flux sensors. During the

measurements, The K-type thermocouple produced slightly higher voltage than K-type, even though T-type thermocouple has a typically slightly higher sensitivity (43 μV/°C) than K-type thermocouple (41 μV/°C) (National Instruments, 2011), although this may be a result of the sensors being slightly misaligned with the laser beam.

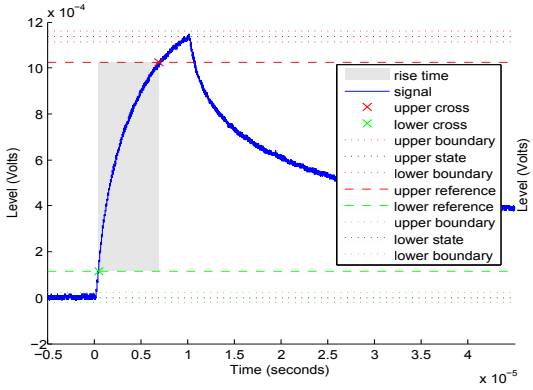

Figure 4.1: B1, response for a 10 μs laser pulse, $t_r = 6.5$ μs.

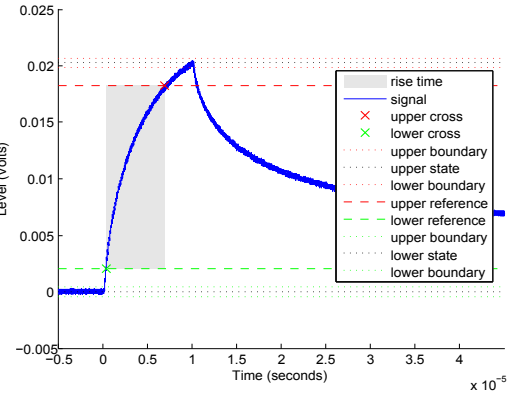

Figure 4.2: B2, response for a 10 μs laser pulse, $t_r = 6.6$ μs.

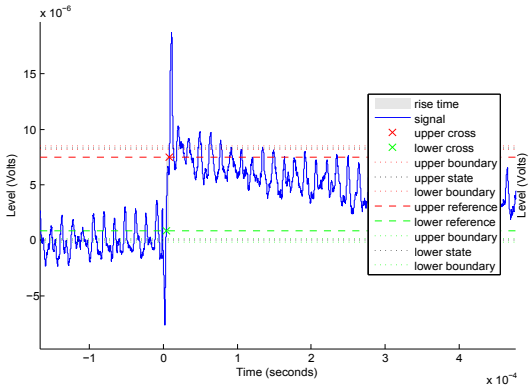

Figure 4.3: HGHFS, response for a 10 μs laser pulse, $t_r \approx 37$ μs. Smoothing with moving average filter, span 2000.

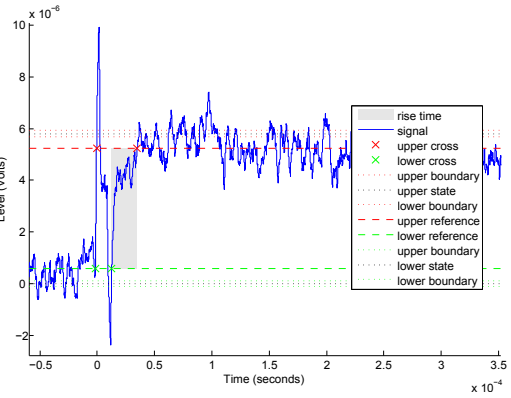

Figure 4.4: HGHFS$_0$, response for a 10 μs laser pulse, $t_r \approx 10$ μs. Smoothing with moving average filter, span 2000.

4.5 Accumulation of heat

The effect of heat build-up in the sensors was studied by subjecting the sensors to 10 μs laser pulses repeated at 9.9 Hz. For the q-sensor, some integration in the output was detected (Fig. 4.5), but the envelope of the output signal reaches its maximum in less that a second (fig. 4.5). The T-sensors' were more strongly affected by the heat accumulation, and increase in output was observed for over 10 seconds.

The PT100 was capable of distinguishing individual laser pulses (fig. 4.5), whereas with the thermocouples, individual pulses were not discerned.
The differing effects of heat accumulation in T- and q-sensors is explained by their working principle. As a q-sensor is heated with pulsed laser, the surface temperature of the sensor rises, forming a temperature gradient along the z-axis of the sensor. This creates thermal $\mathcal{E}$ (eq. 2.12), even if there is no external heat flux present (the laser is turned off between the pulses). Because the output voltage is proportional to the temperature difference across the sensor, the mean temperature or thermal capacity of the sensor body does not affect the output. The T-sensors' output is proportional to the overall temperature of the sensor, and thus directly affected by thermal capacity and accumulated heat.

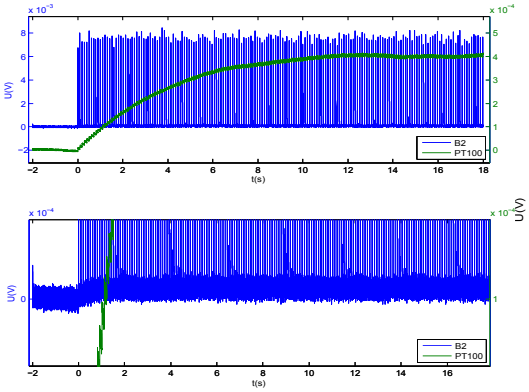

Figure 4.5: Accumulation of heat: output voltages of the sensors B2 and PT100. Stimulation by laser, with pulse duration of 10 μs and repetition rate of 9.9 Hz. Smoothing with moving average filter, span 20.

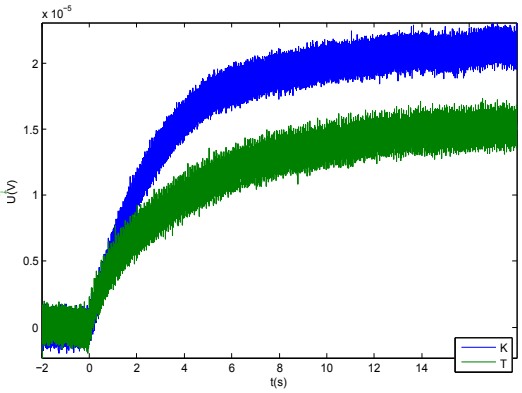

Figure 4.6: Accumulation of heat: output voltages of T- and K-type thermocouples. Stimulation by laser, with pulse duration of 10 μs and repetition rate of 9.9 Hz

4.6 Improving Signal-to-noise ratio

As the time- and voltage resolution of the oscilloscope can be considered accurate, the main cause for measurement error is EMI-related noise. Because of the low output voltage of the sensors, several amplifiers were used in order to improve the signal-to-noise–ratio of the measurement setup. When without amplification, SNR of B1, B2, Si and PT100 was over 1:1, and less than 1:1 with the thermocouples and HGHFS-sensors. Figure 4.7 shows the output of B1-sensor with and without and amplifier. Without amplification, the noise level is approximately 35% of the peak amplitude, and 1.5% with amplifier.

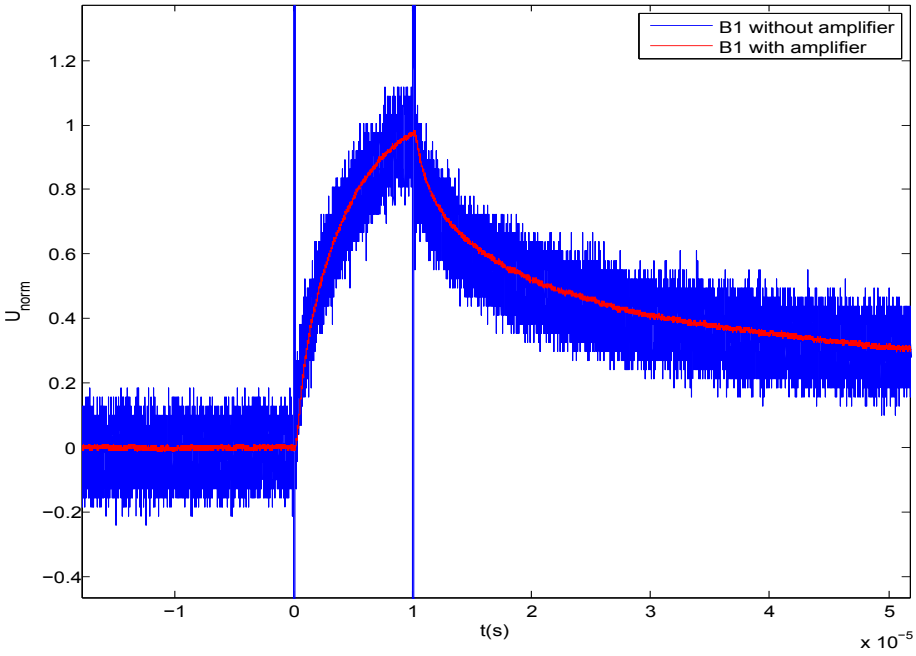

Figure 4.7: Response of B1 to a 10μs laser pulse with and without and amplifier. The output voltages are scaled to match each other.

4.7 Limitations of the measurement setup

In order to measure fast transients, an amplifier must have rise time shorter than the rise time of the sensor to not limit the response time of the setup. The amplifier's step response was measured with 2 mV voltage step from a signal generator, with gain factor set to G=830. The measurements in Fig. 4.8 show a delay time of $t_d = 131$ ns and a rise time of $t_r = 360$ ns. Both t_d and t_r are in the same order of magnitude as the delay times determined for the B1, B2 and Si-sensors. This means that with the amplifier significantly limits the bandwidth when used in conjunction with these sensors, and the actual response times may be shorter.

The measurement setup could be further improved by using a laser capable of providing constant power for a longer period of time ($100 \ldots 1000\mu$s) in order for the sensors to reach steady-state voltage output. With current setup, the determined constants t_d, t_r and t_f depend on the temporal duration of the laser pulse.

The optical setup could be improved by using an optical cable and a focusing lens to provide more consistent exposure for the sensors. The Si-sensor's output's dependence on the sensor's rotational angle suggests that the sensor may be sensitive for the polarization of the laser light. Thus, the experiments should be repeated using a polarizer/analyzer, as no information on the laser's polarization properties was available.

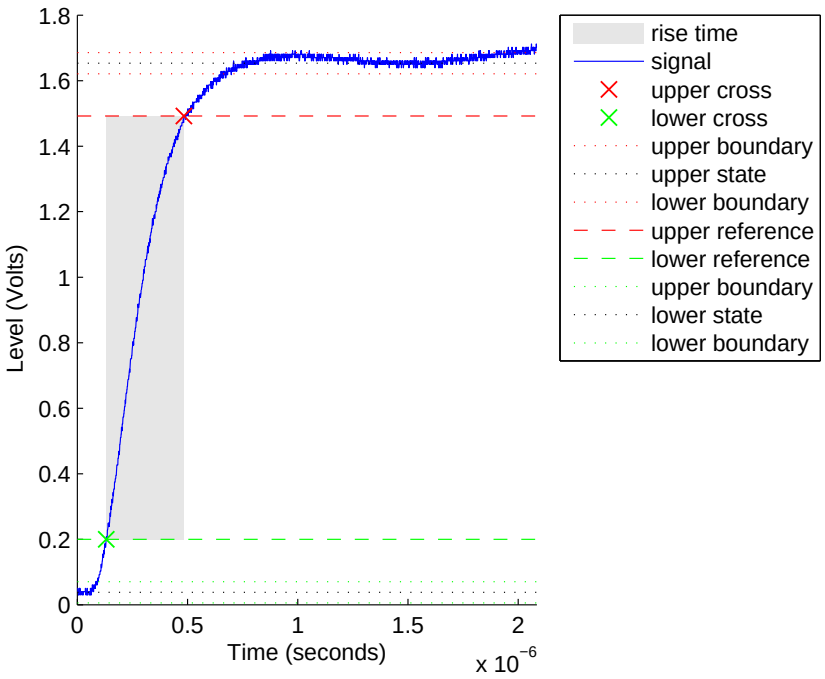

Figure 4.8: Step response of an amplifier with gain G=830

4.8 Comparison with results achieved by others

In our study, the highest volt-watt sensitivity was achieved using silicon-based sensor, followed by bismuth-based sensors. These results agree with Kyarad and Lengfellner (2004), who defined sensitivities for different types of anisotropic thermoelectric devices results, shown in Fig. 4.9:

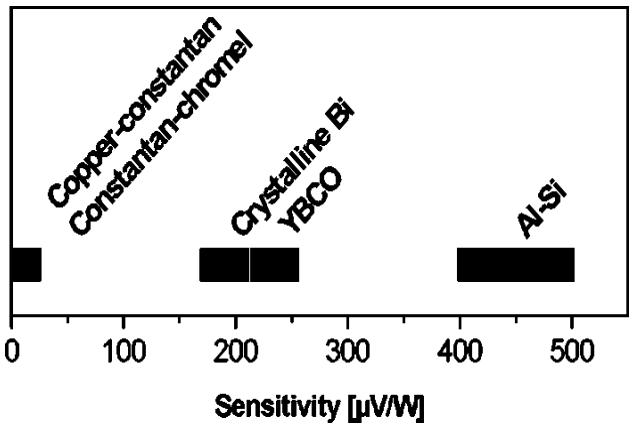

Figure 4.9: Comparison of sensitivity for several light detecting systems based on anisotropic thermoelectricity. (Kyarad and Lengfellner, 2004)

Mityakov's group have suggested a response time of $\sim 10^{-9}$ s for a heat flux sensor stimulated with a 10^{-8} s laser pulse. (Mityakov et al., 2012). Fischer et al. stimulated a q-sensor with a laser diode. A 1 mm-thick sensor based on chromel-constantan multilayers had a response time of ~ 10 ms, and a 0.1 mm-thick sensor had a response time of ~ 100 μs (Fischer et al., 2004). Quin et al. determined rise times between 20 ns and 30 for a heat flux sensor made out of $SrTiO_3/SrTi_{1-x}Nb_xO_3$ multilayer films using 28 ns laser pulses (Qin et al., 2014). These results are similar to those made by us using the bismuth-based sensors, i.e. the rise time is in the same order with the duration of the laser pulse.

The results obtained in this study do not reach the fast responses Mityakov's group achieved. Rise times with q-sensors, however, are under 7 μs with bismuth-based sensors, and in order of 1 μs with the silicon-based sensor. As the bandwidth was limited by the amplifiers used, the true response times are likely even shorter. High-temperature showed slightly longer rise times of approximately 20 μs, probably because of greater thickness or different thermal conductivity of these sensors. There seems to be little correlation between response time and thickness within q-sensors of the same type. The delay- and rise times of bismuth-based sensors did not differ notably from each other, which agrees with the results obtained by Sapozhnikov et al. (2006).

5 Conclusions

Several different types of temperature sensors and heat flux sensors based on transverse Seebeck effect were compared in this study. The sensors were subjected to heat transients generated using a pulsed diode laser, and delay, rise, and fall times were defined for each sensor. It was observed that the heat flux sensors have significantly faster response to a laser pulse (~ 10 μs) than the temperature sensors (~ 1000 μs). Differences in response times and volt–watt sensitivities between different types of heat flux sensors and temperature sensors were also observed. Because of low output voltage of the sensors, amplifiers were used to improve the signal-to-noise ratio of the measurement setup. However, it was observed that the amplifiers used limit the bandwidth of the sensors, and true response times may be shorter.

5.1 Future work

The Gradient Heat Flux Sensor provides only millivolts of output voltage, so amplification and EMI-shielding is required in order to obtain accurate information about small changes in heat flux. The response experiments in this work should be redone using a heat source with longer continuous output to obtain proper step responses from the sensors. The amplifier should also be re-designed in such a way that the bandwidth of the sensor is not being limited.

References

(2015). *PT100 platinum resistance thermometers*. url: https://www.picotech.com/library/application-note/pt100-platinum-resistance-thermometers.

Bobashev, S., et al. (2008). Application of the gradient heat flux sensor to study pulsed processes in a shock tube. *Technical Physics*, 53(12), pp. 1634–1635. ISSN 1063-7842, doi:10.1134/S1063784208120189, url: http://dx.doi.org/10.1134/S1063784208120189.

Boydston, R.W. (1927). Thermo-electric Effect in Single-Crystal Bismuth. *Physical Review, volume 30*.

Domenicali, C.A. (1953). Irreversible Thermodynamics of Thermoelectric Effects in Inhomogeneous, Anisotropic Media. *Phys. Rev.*, 92, pp. 877–881. doi:10.1103/PhysRev.92.877, url: http://link.aps.org/doi/10.1103/PhysRev.92.877.

Fischer, K., Stoiber, C., Kyarad, A., and Lengfellner, H. (2004). Anisotropic thermopower in tilted metallic multilayer structures. *Applied Physics A*, 78(3), pp. 323–326. ISSN 0947-8396, doi:10.1007/s00339-003-2326-y, url: http://dx.doi.org/10.1007/s00339-003-2326-y.

Goldsmid, H.J. (2010). *Introduction to Thermoelectricity*. Springer.

Heiskanen, T. (2015). *Design and implementation of measurement electronics for heat flux sensor*. Master's thesis. Lappeenranta University of Technology.

Jussila, H., et al. (2013). Local Heat Flux Measurement in a Permanent Magnet Motor at No Load. *Industrial Electronics, IEEE Transactions on*, 60(11), pp. 4852–4860. ISSN 0278-0046, doi:10.1109/TIE.2012.2222853.

Kanno, T., et al. (2014). Detection of Thermal Radiation, Sensing of Heat Flux, and Recovery of Waste Heat by the Transverse Thermoelectric Effect. *Journal of Electronic Materials*, 43(6), pp. 2072–2080. ISSN 0361-5235, doi:10.1007/s11664-013-2959-3, url: http://dx.doi.org/10.1007/s11664-013-2959-3.

Kyarad, A. and Lengfellner, H. (2004). Al-Si multilayers: A synthetic material with large thermoelectric anisotropy. *Applied Physics Letters*, 85(23), pp. 5613 – 5615. ISSN 00036951, url: http://search.ebscohost.com/login.aspx?direct=true&db=afh&AN=15305399&site=ehost-live.

Lienhard IV, J.H. and Lienhard V, J.H. (2015). *A Heat Transfer Textbook, 4th edition*. Phlogiston Press, Cambridge, Massachusetts, USA.

Mann, B.S. (2006). *Transverse Thermoelectric Effects for Cooling and Heat Flux Sensing*. Master's thesis. Virginia Polytechnic Institute and State University, Blacksburg, Virginia.

Mityakov, A.V., et al. (2012). Gradient heat flux sensors for high temperature environments. *Sensors and Actuators A: Physical*, 176, pp. 1 – 9. ISSN 0924-4247, doi: http://dx.doi.org/10.1016/j.sna.2011.12.020, url: http://www.sciencedirect.com/science/article/pii/S0924424711007187.

National Instruments (2011). *Tables of Thermoelectric Voltages for All Thermocouple Types*. url: http://www.ni.com/white-paper/4231/en/.

Niukkanen, M. (2013). *Design of an amplifier and an instrumentation setup for a harsh environment heat flux measurement application - case axial flux electric machine*. Master's thesis. Lappeenranta University of Technology.

Qin, Y., et al. (2014). Development of a transverse thermoelectric voltage effect in artificial SrTiO3/SrTi1-xNbxO3 epitaxial multilayer films with incline-oriented sublayers. *CrystEngComm*, 16, pp. 5345–5351. doi:10.1039/C4CE00170B, url: http://dx.doi.org/10.1039/C4CE00170B.

Reitmaier, C., Walther, F., and Lengfellner, H. (2010). Transverse thermoelectric devices. *Applied Physics A*, 99(4), pp. 717–722. ISSN 0947-8396, doi:10.1007/s00339-010-5742-9, url: http://dx.doi.org/10.1007/s00339-010-5742-9.

Sapozhnikov, S., Mityakov, V., and Mityakov, A. (2006). Gradient heat-flux sensors: Possibilities and prospects of use. *Thermal Engineering*, 53(4), pp. 270–278. ISSN 0040-6015, doi:10.1134/S0040601506040033, url: http://dx.doi.org/10.1134/S0040601506040033.

Sapozhnikov, S., Mityakov, V., Mityakov, A., and Mozhaiskii, S. (2008). Gradient-type sensors for heat flux measurements high temperatures. *Technical Physics Letters*, 34(10), pp. 815–817. ISSN 1063-7850, doi:10.1134/S1063785008100015, url: http://dx.doi.org/10.1134/S1063785008100015.

Sapozhnikov, S., et al. (2012). The calibration of gradient heat flux sensors. *Measurement Techniques*, 54(10), pp. 1155–1159. ISSN 0543-1972, doi:10.1007/s11018-012-9864-7, url: http://dx.doi.org/10.1007/s11018-012-9864-7.

Scervini, M. (2009). *Thermocouple: The Operating Principle*. url: http://www.msm.cam.ac.uk/utc/thermocouple/pages/ThermocouplesOperatingPrinciples.html.

Snarskii, A.A., Palti, A.M., and Ashcheulov, A.A. (1997). Anisotropic thermocouples article. *Semiconductors*, 31(11), p. 1101. ISSN 10637826, url: http://search.ebscohost.com/login.aspx?direct=true&db=afh&AN=7318486&site=ehost-live.

Sujay, R.M. (2005). *Design and Calibration of a Novel High-Temperature Heat Flux Sensor*. Master's thesis. Virginia Polytechnic Institute and State University, Blacksburg, Virginia.

Tunnell, J., Torres, J., and Anvari, B. (2002). Methodology for Estimation of Time-Dependent Surface Heat Flux due to Cryogen Spray Cooling. *Annals of Biomedical Engineering*, 30(1), pp. 19–33. ISSN 0090-6964, doi:10.1114/1.1432691, url: `http://dx.doi.org/10.1114/1.1432691`.

Vemuri, K.P. and Bandaru, P.R. (2013). Geometrical considerations in the control and manipulation of conductive heat flux in multilayered thermal metamaterials. *Applied Physics Letters*, 103(13), pp. 133111 – 133111–4. ISSN 00036951, url: `http://search.ebscohost.com/login.aspx?direct=true&db=afh&AN=90480415&site=ehost-live`.

Young, H.D. and Freedman, R.A. (2008). *University Physics with Modern Physics*. Pearson Education. ISBN 9788131717967.

Zahner, T., Stoiber, C., Zepezauer, E., and Lengfellner, H. (1999). Transverse Thermoelectricity in a Tilted Metallic Multilayer Structure. *International Journal of Infrared and Millimeter Waves*, 20(6), pp. 1103–1111. ISSN 0195-9271, doi:10.1023/A:1021720422114, url: `http://dx.doi.org/10.1023/A%3A1021720422114`.

A Appendix

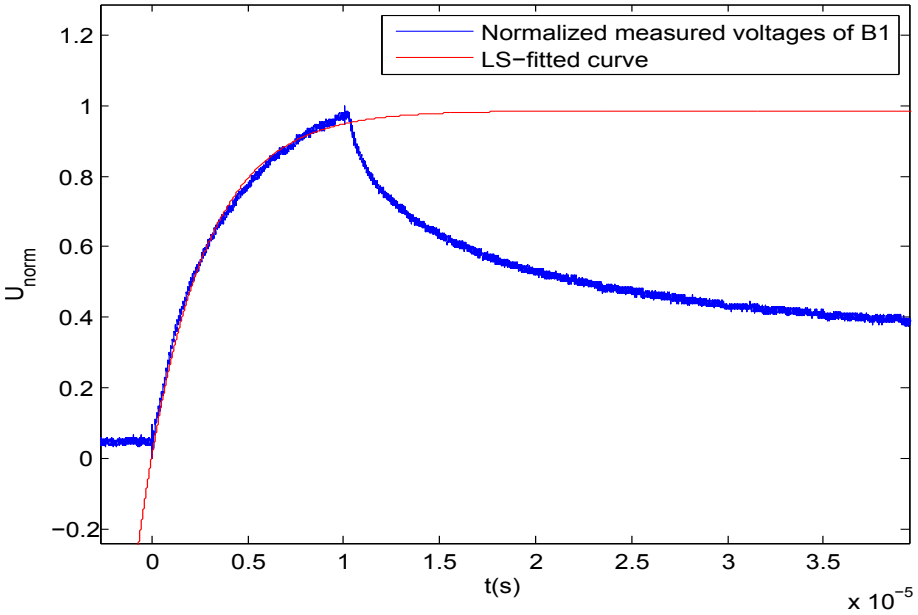

Figure A.1: B1: normalized response for 10 μs laser pulse and fitted 1st order system step response curve

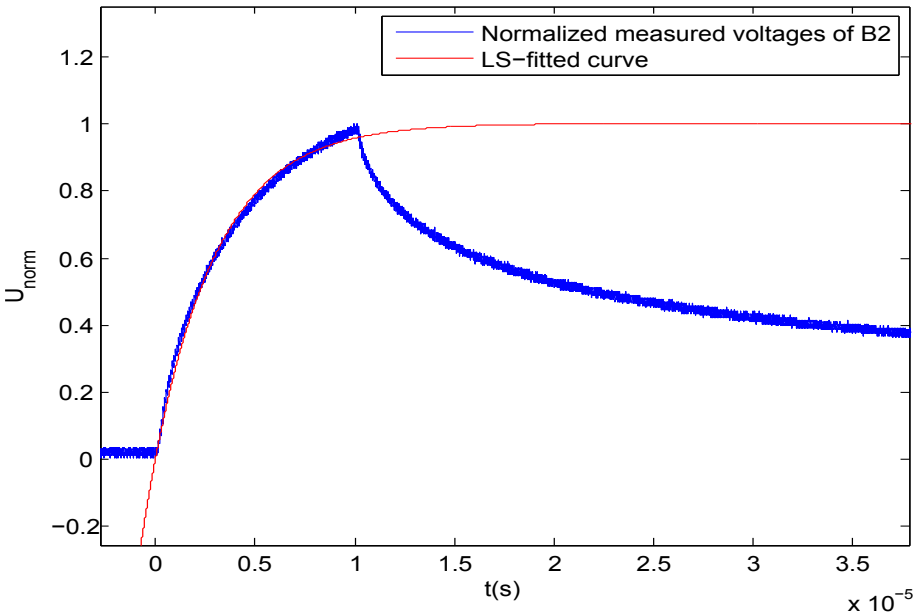

Figure A.2: B2: normalized response for 10 μs laser pulse and fitted 1st order system step response curve